Evaluation of Algebraic Iterative Algorithms for Reconstruction of Electron Magnetic Resonance Images

S.Sivakumar	Murali C.Krishna	R.Murugesan
C.P.A.College	National Cancer Institute	Madurai Kamaraj University
Bodinayakanur 625 513	Bethesda, Maryland 20812	Madurai 625 021
sivaku2002@yahoo.com	murali@helix.nih.gov	rammku@eth.net

Abstract

Electron Magnetic Resonance Imaging (EMRI) is emerging as a potential tool for noninvasive imaging of free radicals in biological systems. The EMR images are generally reconstructed using the filtered back projection (FBP) method, because of its speed and simplicity. But, the FBP method fails when reconstruction is attempted with limited number of projections or with noisy projections. In addition, it also suffers due to star artifact. Iterative algorithms such as additive algebraic reconstruction technique (AART), multiplicative algebraic reconstruction technique (MART) form another major class of tomographic reconstruction methods. These methods are known to give artifact free imaging with minimal number of projections in computerized tomography (CT), positron emission tomography (PET) and single photon emission tomography (SPECT). In this paper, the application of algebraic iterative reconstruction methods for reconstruction of EMR image is critically evaluated. Both phantom and in vivo*EMR images are reconstructed using projection data collected from a radio frequency (RF) continuous wave (CW) EMR imager. Both visualization and computation of signal to noise ratio (SNR) are used to evaluate the performance of the methods. Nine different reconstruction methods viz. Brooks, Mayinger, Gordon, Gilbert and Anderson AART methods and four MART methods are compared. Among these methods, Mayinger method, a variant of AART performs better than the other methods.*

1. Introduction

Tomographic image reconstruction has been an active research area in recent years. Image reconstruction is performed in a computer with different types of reconstruction algorithms [5, 1]. Reconstruction methods utilize projection data as input and produce estimates of the original internal structure as output [14, 17]. FBP and algebraic model based iterative algorithms are the two major classes of reconstruction methods. The FBP method is widely used for different imaging modalities such as CT and PET in clinical settings because of its speed and easy implementation. EMR imaging is a newly evolving technique that can directly detect, characterize and quantify free radicals in chemical and biological systems. Functional EMR studies have been carried out in small animals to probe parameters of physiological importance, such as tissue metabolic activity, redox status and oxygen concentration [12, 10]. In EMR imaging projections are collected by sweeping the magnetic field at projection angles defined by the magnetic field gradient directions [16, 13]. To perform image reconstruction , the projections $p_o(r)$, collected along a set of field-gradient orientations in polar coordinates, are used to obtain the sample electron spin density $f(x, y)$ by FBP,

$$f(x,y) = \int_0^{\pi} p^*_\theta(r) d\theta = \int_0^{\pi} [\int_{-\infty}^{\infty} P_\theta(k)|k|e^{-2\pi ikr} dk] d\theta, \quad (1)$$

Here r is taken on the x-y plane such that $r = xcos\theta + ysin\theta$, and $p^*_\theta(r)$ is the projection $p_\theta(r)$ filtered according to the expression inside the square brackets.

Although EMRI is akin to the well known magnetic resonance imaging (MRI) for biomedical applications EMRI techniques require the incorporation of a suitable paramagnetic imaging agent (spin probe) into the system under investigation. To avoid toxicity, the imaging agents are to be administered in small dose which results in noisy projections. In addition, long projection data collection time must be avoided to cope up with the biological clearance of the imaging agents. Under such conditions only limited number of projections may be collected. The potential of EMRI depends on the ability of reconstruction algorithms to generate artifact free images from the limited number of projection measurements. For noisy projection data as well as for limited number of projections, the FBP method of image of reconstruction shows very poor performance. Hence currently there is considerable interest to evaluate the use of other reconstruction methods for EMR images [3, 8, 7, 2, 9, 15].

An iterative method using a non-linear fit to the projection data has shown to give ripple free images [3]. Fourier reconstruction (FR) method used to obtain two-dimensional

EMR image from a set of one-dimensional projections requires elimination of different phase errors [8]. Recently, the application of maximum entropy reconstruction methods to EMR imaging has been explored [7]. In this study, EMR images of two physical phantoms, reconstructed using FBP, multiplicative algebraic reconstruction technique (MART) and least square entropy (LSEnt) were compared. The results of phantom study have shown encouraging indication of the potential of maximum entropy reconstruction methods of EPR images. In general, the iterative reconstruction techniques perform better than the FBP method when reconstruction is attempted with limited number of projection data. Here we report the evaluation of two major groups of ART methods, namely additive ART (AART) and multiplicative ART for EMRI, using phantom as well as in vivo EMR measurements. Various types of correction sequences on the AART and MART, leading to nine sub groups of algorithms are tested for their performance for successful reconstruction of EMR images from limited number of projection data and compared with the FBP method.

2. EMR Imaging

2.1. EMR Projection Data Collection

EMR projection data were acquired using a RF CW EMR imager that operates at a nominal frequency of 300 MHz, corresponding to a resonant magnetic field of 106 G (10.6 mT) for $g = 2$ spin systems. A full description of the EMR imager is presented elsewhere [11]. A home-built parallel coil resonator (25 mm x 25 mm) was used for EMR data collection. Two derivatives of symmetric trityl based free radicals, abbreviated as Oxo63 and Oxo31 were used as exogenous imaging agents [13]. The imaging experiments were carried out as per the procedure reported earlier [16, 13].

2.2. Phantom Imaging

To evaluate the performance of the various algorithms a lucite cylindrical phantom with 17 holes of 3.3 mm diameter, drilled parallel to the axis of the cylinder was used. The center to center distances of the holes in the outer circle and the inner circles are 7.3 mm and 3.6 mm respectively. Each hole of the phantom was filled with 150 μL of 1 mM solution of the imaging agent, Oxo31.

2.3. In vivo Imaging

The EMRI experiments involving animals were performed in accordance with the guide for the care and use of laboratory animals prepared by the institute of laboratory animal resources, National Research Council. A C3H mouse was anesthetized (i.p. or i.v.) with a mixture of ketamine (90 mg/kg of body weight) and xylazine (30 mg/kg of body weight) and placed (lying on its back) in a parallel coil resonator. The image sequence was generated after intravenous injection of the imaging agent, (100-200 μL of a 10 mM solution of Oxo63 in PBS) by tail-vein cannulation. The projection data were collected from the CW EMR imager at different time intervals during the EMR imaging process.

3. Image Reconstruction

In CW EMR imaging, tomographic projections are collected in a polar grid by sweeping the magnetic field at projection angles defined by the static magnetic field gradient directions. In the multiple gradient approach of EMR imaging, stepped gradients are used to generate projections of a sample at various angles. Data sets with 36 projections measured from 0^o to 180^o around the object were considered for the phantom study. The same data set was used for testing the capability of the algorithms from limited number of projections, by skipping projections at uniform angular distribution. For in vivo studies, data sets with only 18 projections could be measured. Each projection was sampled to 128 points. The object is made of 128*128 pixels whose values give the amount of paramagnetic contrast material inside the object. The flowchart in Figure 1 shows the procedure for the reconstruction of EMR images using iterative algebraic reconstruction algorithms. The system was implemented using MATLAB coding. The classical iterative reconstruction technique is the algebraic reconstruction tech-

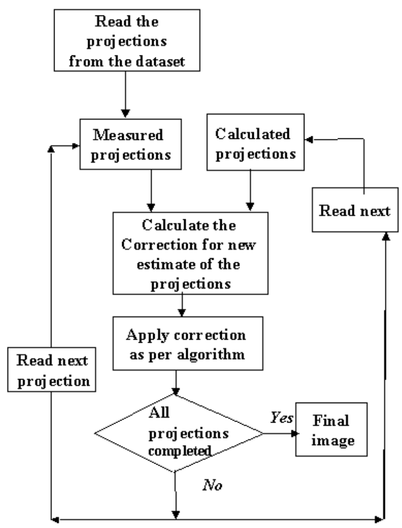

Figure 1: Flowchart of the iterative algebraic image reconstruction system

nique (ART) in which systematic refinements are made to an initial estimate of the object, so that the refined estimate remains consistent with each set of projection data. ART is an efficient method, because it incorporates corrections during the iterations, without a significant increase in computation time. Ideally the image, f(**x,y**) is a continuous two dimensional function and an infinite number of projections are required for reconstruction. In practice$f$(**x,y**) is calculated using a finite number of points $fi(i = 1, 2, 3, ..., N)$ (samples) from a finite number of projections. The spectral profile of the sample for various projections are not ideal lines but have a 'finite width'. The sample sums are made up of contributions from each cell intersected by the sample. For example, for the j^{th} sample, the sum is given by

$$fi = W_{1j}f_1 + W_{2j}f_2 + W_{3j}f_3 + \ + W_{nj}f_n \qquad (2)$$

Equation (2) can be replaced by the following set of algebraic equations

$$P_j = W_{1j}f_1 + W_{2j}f_2 + \ + W_{nj}f_n$$

$$P_j = \sum W_{ij}f_j, i = 1, 2, ..., M \qquad (3)$$

Here W_{ij} is the weighting factor that represents the contribution of the i^{th}cell to the j^{th} sample sum and P_j represents a set of matrix equations for the data points f_j. Direct solution of equation(3) is generally not practical because of the large number of cells. Hence the density values f_j are iteratively adjusted until the calculated projections agree with the measured projections. The general procedure used in the iterative reconstruction method is as outlined below.

1. The cell densities are initialized with $f_j = 0$ for blank screen and $f_j =$ for gray screen.
2. From the initial densities the projections are calculated using equation(1).
3. The calculated projections have been compared with the measured projections.
4. If, calculated sample sum = measured value, for all cells and all samples the first iteration is completed else, errors still exist.
5. This procedure is repeated until the remaining error is within acceptable limits.
6. The corrections are applied to all cells along the sample, instead of selectively being applied to cells that need corrections, because cells needing corrections are not known *a priori*.

   Mathematically the correction process during l^{th} iteration is described by the equation, $f_i^l = f_i^{l-1} + \Delta f_{ij}^l$ Here f_i^{l-1} is the density before the iteration, f_i^l is the density after the iteration and Δf_{ij}^l is the correction applied to the i^{th} cell from the j^{th} sample.

4. Additive ART

In ART, at the start of each iteration one sample sum is calculated and corrections are applied to all points that contribute to the sample. When the correction terms are additive, the procedure is called additive ART (AART). The general algorithm of AART is as follows. For each projection angle θ

1. For each sample i_θ the correction term is computed. During the l^{th} iteration, the l^{th} calculated value, P_j^c is compared with the measured value P_j, and the error is estimated from $\Delta P_j = P_j - P_j^c$.
2. The correction coefficient $\alpha_i = \sum_{j=1}^{N} W_{ij}^2$ is computed.
3. Then the average value of correction $\overline{\Delta P_j} = W_{ij}\frac{\Delta P_j}{\alpha_i}$ is calculated.
4. Steps 1 to 3 are repeated for all samples.
5. Correction is applied for each cell j, $f_i^l = f_i^{l-1} + \lambda\overline{\Delta P_j}$ where λ is the relaxation parameter
6. Step 5 is repeated for all the samples of a projection angle θ.

4.1. Various Types of ART

Variations in the sequence in which corrections are made leads to different types of AART. In the present study five different types of correction formulae have been applied to the additive ART procedure. These different types of AART algorithms are described below.

Brooks has proposed the ART algorithm with additive correction [1]. Let P_j^c be the projection due to the i^{th} sample with magnetic field gradient distribution and $\overline{f_i}$ be the initial assumption. The approximated (calculated) projection due to the test field is

$$P_j^c = \sum_{j=1}^{N} W_{i_\theta j} f_j, i_\theta = 1, 2, ..., M_\theta \qquad (4)$$

Here i_θ denotes the i^{th} sample corresponding to projection angle θ. Mayinger has suggested the simplest AART [15]. For each projection angle the total value of the weight function is computed. Gordon has proposed the ART algorithm [9] with additive correction. In this method, corrections are applied to all the cells through which the i^{th} sample passes, before calculating the correction for next sample. Hence the number of samples per projection angle is not important as in equation(3). Gilbert has developed an AART algorithm [14] in which the elements of the field function are modified after the calculation of all the correction values corresponding to individual samples. Anderson and Kak have proposed a new algorithm, which combines the ART and simultaneous iterative reconstruction technique (SIRT) algorithms [15]. The method of applying a correction is similar to Mayinger AART, but the structure is similar to AART. The correction term for the various additive ART methods are as follows.

Brooks AART: $\alpha_i = \sum_{j=1}^{N} W_{ij}^2$

Mayinger AART: $W_{i_\theta} = \sum_{j=1}^{N} W_{i_\theta j}$

Gordon AART: $\alpha_i = \sum_{j=1}^{N} W_{ij}^2$

Gilbert AART: $\alpha_i = \sum_{j=1}^{N} W_{ij}^2$

Anderson AART: $\alpha_{i_\theta} = \sum_{j=1}^{N} W_{i_\theta j}^2$

5 Multiplicative ART

When the correction is multiplicative the ART is called multiplicative ART (MART). The initial approximate projection is computed using equation (2). The general algorithm of MART is as follows.

For each iteration l

1. The calculated value P_j^c is approximated for each sample i.
2. All samples passing through a given cell were identified. The total number of samples per cell NC_j corresponds to i, W_{ij}, P_j, P_j^c.
3. The product of all correction terms are computed for each cell j.

This completes the l^{th} iteration.

In the work presented here, Brooks multiplicative correction and three other types of correction techniques have been evaluated for EMR image reconstruction.The correction term can be accomplished in four different ways as given below.

Brooks MART: $f_i^l = f_i^{l-1} + \prod_{NC_j} [\lambda W_{ij} (\frac{P_j}{P_j^c})]$

MART method1: $f_i^l = f_i^{l-1} + \prod_{NC_j} [1 - \lambda(1 - \frac{P_j}{P_j^c})]$

MART method2: $f_i^l = f_i^{l-1} + \prod_{NC_j} [1 - \lambda W_{ij} (1 - \frac{P_j}{P_j^c})]$

MART method3: $f_i^l = f_i^{l-1} + \prod_{NC_j} [\frac{P_j}{P_j^c}]^{\lambda W_{ij}}$

6. Results and Discussion

It is well known that the phantom imaging is a standard method to compare and test different reconstruction algorithms. In the present work, two different data sets, one comprising of a phantom object and the other of in vivo mouse are used to evaluate the reconstruction methods in terms of image quality and reconstruction time.

6.1. Phantom Imaging

Schematics (not to scale)of the 17-tube phantom is shown in figure 2. Transverse spatial EMR images of the 17-tube

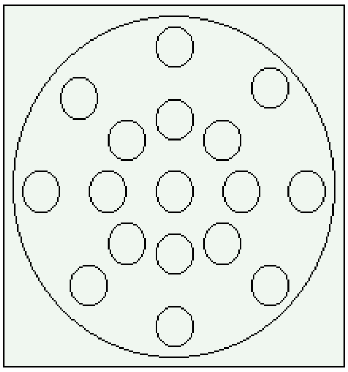

Figure 2: Sketch (not to scale) of the cylindrical 17-tube phantom.

phantom reconstructed by FBP and the additive ART algorithms are shown in figure 3.In this figure, rows 1, 2, 3 and 4 refer to images reconstructed using 36, 18, 12 and 4 number

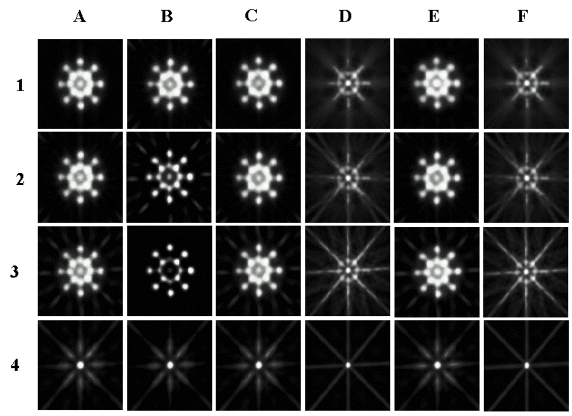

Figure 3: EMR images of the 17-tube phantom reconstructed by FBP and AART methods.

of projections respectively. Similarly columns **A**, **B**, **C**, **D**, **E**, **F** refer to the images reconstructed using FBP, Brooks, Mayinger, Gordon, Gilbert and Anderson AART methods respectively. From these results it is seen that for 36 and 18 projections (**A**)FBP, (**C**)Mayinger and (**E**)Gilbert algorithms show almost comparable performance. Both Gordon and Anderson methods show large streak artifacts. Although performance of (**B**)Brooks algorithm gets poor as the number of projections becomes small, it does not show significant artifacts. On the other hand it shows better resolution.

For the same phantom the EMR images reconstructed using MART algorithms are presented in figure 4. Here also rows 1, 2, 3 and 4 correspond to images reconstructed

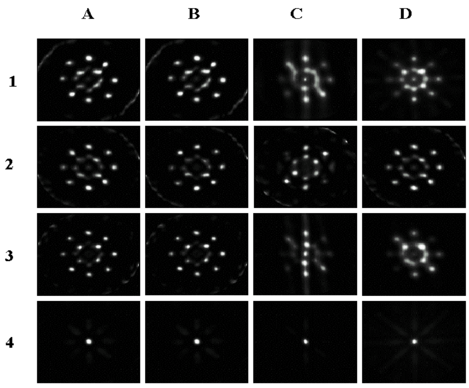

Figure 4: EMR images of 17-tube phantom reconstructed by MART methods.

using 36, 18, 12 and 4 projections respectively. However, columns **A**, **B**, **C**, **D** refer to the reconstruction algorithms Brooks MART (**A**), method1(**B**), method2(**C**) and method3(**D**) MART methods respectively. On visualization of the images it is inferred that the MART methods perform very poor compared to the AART methods.

6.2. Renal Imaging

In vivo EMR images of a C3H mouse reconstructed by FBP and all other additive ART algorithms are shown in figure 5. For this study, projections (128 samples), collected at 2.8

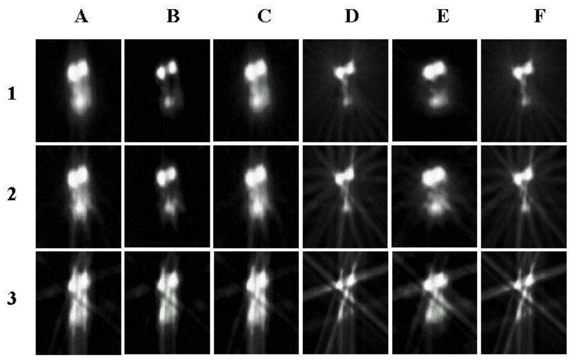

Figure 5: EMR images of a C3H mouse reconstructed by AART methods.

minutes after the administration of the imaging agent were used. The EMR images show the distribution of imaging agent predominantly in the kidneys (top) and bladder (bottom). Rows 1, 2 and 3 refer to images reconstructed using 18, 9 and 4 projections respectively. Similarly column **A**, **B**, **C**, **D**, **E**, **F** refer to the images reconstructed using FBP, Brooks, Mayinger, Gordon, Gilbert and Anderson AART methods respectively. For the same mouse the images reconstructed using MART algorithms are presented in figure 6. Here also rows 1, 2 and 3 correspond to images reconstructed using 18, 9 and 4 projections respectively. However, columns **A**, **B**, **C**, **D** refer to images reconstructed using Brooks MART(**A**), MART method1(**B**), method2(**C**) and method3(**D**) respectively.

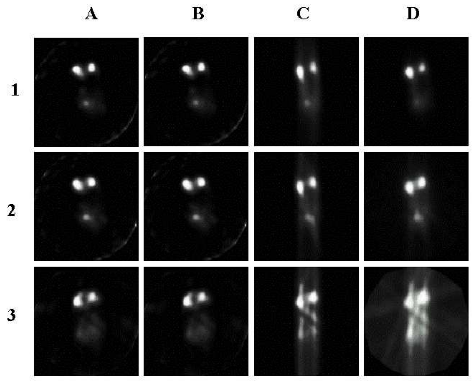

Figure 6: EMR images of a C3H mouse reconstructed by MART methods.

The performance of the various algorithms for *in vivo* image reconstruction is comparable to the phantom study. In addition to visual analysis, calculation of the signal to noise ratio (SNR) serves as a useful measure of image quality. A method for quantitative evaluation of image quality has been proposed [4, 6]. The standard SNR measure is the mean signal in a region of interest (ROI) over standard deviation of noise in the same ROI. Uniformity of image SNR is the variation of image SNR over one imaging plane. Following this procedure SNR values were calculated for the in vivo EMR images. These values are listed in Table 1. Of the various methods Mayinger ART shows the largest SNR values computed for the kidneys.

Method	LeftKidney	RightKidney	Bladder
FBP	9.99	8.99	12.59
Brooks ART	7.75	7.68	7.03
Mayinger ART	13.12	10.99	13.65
Gordon ART	11.1	9.27	10.06
Gilbert ART	13.39	9.24	7.79
Anderson ART	9.02	9.08	8.31
Brooks MART	3.23	3.95	4.22
MART method1	5.14	6.21	2.97
MART method2	5.49	4.94	6.88
MART method3	5.29	3.91	3.87

Table 1: Quality measure(SNR in db) of an *in vivo* EMR image for the reconstruction methods with 18 projections

Reconstruction times taken by the various iterative algebraic methods, evaluated in an IBM Intellistation Computer (model 6214, Intel(R) Pentium IV, 1.60 GHz 128 MB RAM) under Windows 2000 platform for in vivo EMR images are presented in figure 7. At present no attempt has been made to optimize the MATLAB codes for performance.

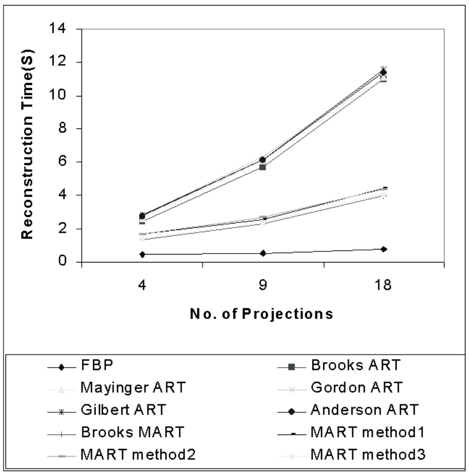

Figure 7: Time complexity of the reconstruction methods with respect to number of projections

7. Conclusion

Results of EMR image reconstruction from projection data using various algebraic iterative methods and FBP method are presented. In general the AART methods show better SNR and better resolution in comparison to the MART methods. Of the various AART iterative methods evaluated, the Mayinger AART showed the best performance. The reconstruction time shows clear distinction between the iterative methods and the traditional FBP method. Next to FBP Brooks ART shows the low time complexity. Investigation of the effect of various types of noise in the projection data on the performance of the reconstruction algorithms in progress.

References

[1] R. A.Brooks and G. D. Chiro. Theory of image reconstruction in computed tomography. *Radiology*, 117, December 1975.

[2] C.A.Johnson, J.A.Cook, D.McGarry, N.Devasahayam, J.B.Mitchell, S.Subramanian, and M.C.Krishna. Maximum entrophy reconstruction methods in electron paramagnetic resonance imaging. *Annals of Operations Research*, 119, January 2003.

[3] C.N.Smith and A.D.Stevens. Reconstruction of images from radiofrequency electron paramagnetic resonance spectra. *The British Journal of Radiology*, 67, 1994.

[4] M. Fuderer. The information content of mr images. *IEEE Transactions on Medical Imaging*, 7(4), December 1983.

[5] G.L.Zeng. Image reconstruction a tutorial. *Computerized Medical Imaging and Graphics*, 25, 2001.

[6] G.McGibney and M.R.Smith. An unbiased signal to noise ratio measure for magnetic resonance images. *Medical physics*, 20(4), July/August 1993.

[7] G.Placidi, M.Alecci, and A.Sotgiu. Fourier reconstruction as a valid alternative to filtered back projection in iterative applications: Implementation of fourier spectral spatial epr imaging. *Journal of Magnetic Resonance*, 134, 1998.

[8] G.Placidi, M.Alecci, G.Gualtieri, and A.Sotgiu. Optimization of electron paramagnetic resonance image reconstruction using filtered back projection followed by two dimensional deconvolution. *Journal of Magnetic Resonance*, A121, March 1996.

[9] G. T. Herman and A. Lent. Iterative reconstruction algorithms. *Computers in Biology Medicine*, 6, January 1976.

[10] H.Yokoyama and et al. A Spatiotemporal Study on the Distribution of Intraperitoneally Injected Nitroxide Radical in the Rat Head Using an *in vivo* esr Imaging system. *Magnetic Resonance Imaging*, 14, 1996.

[11] J.Koscielniak, N.Devasahayam, M.S.Moni, P.Kuppusamy, K.Yamada, J.B.Mitchell, M.C.Krishna, and S.Subramanian. 300 mhz continuous wave electron paramagnetic resonance spectrometer for small animal in vivo imaging. *Review of Scientific Instruments*, 71(11), November 2000.

[12] P. Kuppusamy and M. C. Krishna. Epr Imaging of Tissue Redox Status. *Current topics in Biophysics*, 26(1), 2002.

[13] K.Yamada, R.Murugesan, N.Devasahayam, J.A.Cook, J.B.Mitchell, S.Subramanian, and M.C.Krishna. Evaluation and comparision of pulsed and continuous wave radiofrequency electron paramagnetic resonance techniques for in vivo detection and imaging of free radicals. *Journal of Magnetic Resonance*, 154, 2002.

[14] P.F.C.Gilbert. Iterative methods for the three dimensional reconstruction of an object from projections. *Journal of Theor. Biology*, 36, July 1972.

[15] P.M.V.Subbarao, P.Munshi, and K.Muralidhar. Performance of iterative tomographic algorithms applied to non destructive evaluation with limited data. *NDT and E International*, 30, 1997.

[16] R.Murugesan, M.Afeworki, J.A.Cook, N.Devasahayam, R.Tschudin, J.B.Mitchell, S.Subramanian, and M.C.Krishna. A broadband pulsed radio frequency electron paramagnetic resonance spectrometer for biological applications. *Review of Scientific Instruments*, 69(4), April 1998.

[17] S.Vandenberghe, Y.D.Asseler, R.Vandewalle, T.Kauppinen, M.Koole, L.Bouwens, K. Laere, I.Lemahieu, and R.A.Dierckx. Iterative reconstruction algorithms in nuclear medicine. *Computerized Medical Imaging and Graphics*, 25, 2001.